Indian Institute of Technology, Bombay

Airfoil Analysis Report

Prepared by: Atul Krishna
Roll No: 22B0071

Aerodynamics Laboratory-AE343
-Prof. Vineet Nair

Contents

List of Figures

List of Tables

List of Symbols

α Angle of Attack

C_a Sectional coefficient of force along free-stream direction

C_l Sectional coefficient of Lift calculated from experimental data

C_n Sectional coefficient of force along the direction normal to free-stream direction

$C_{d,f}$ Sectional coefficient of skin-friction Drag calculated from experimental data

$C_{d,p}$ Sectional coefficient of Pressure Drag calculated from experimental data

$C_{d,total}$ Sectional coefficient of Total Drag calculated from experimental data

$C_{l,th}$ Theoretical sectional coefficient of Lift obtained from the Thin Airfoil Theory

$C_{m,c/4,th}$ Theoretical sectional coefficient of Quarter Chord Moment obtained from the Thin Airfoil Theory

$C_{m,c/4}$ Theoretical sectional coefficient of Quarter Chord Moment calculated from experimental data

$C_{m,LE,th}$ Theoretical sectional coefficient of Leading Edge Moment obtained from the Thin Airfoil Theory

$C_{m,LE}$ Theoretical sectional coefficient of Leading Edge Moment calculated from experimental data

x_{ac} Aerodynamic Center

x_{cp} x Coordinate Center of pressure

z_l z coordinates of Lower Surface of the Aerofoil

z_u z coordinates of Upper Surface of Aerofoil

1 Abstract

- The experiment focused on observing and analyzing the behavior of low-speed airflow over a symmetric airfoil at high Reynolds numbers.
- Lift, drag, and moment characteristics were calculated for different angles of attack.
- The variations in these characteristics were determined numerically and then compared with theoretical and existing computational data.
- The aerodynamic center (x_{ac}) was predicted based on the collected data and compared with both theoretical and experimental results from literature.
- The estimated drag and lift coefficients closely aligned with theoretical values.
- However, the moment coefficients displayed significant deviations from theoretical predictions at high angles of attack.
- This discrepancy was attributed to the breakdown of basic assumptions like minimal flow perturbation and thin airfoil theory.

2 Objectives

- To predict the sectional lift coefficients (C_l), pitching moments about the quarter chord point ($C_{m,c/4}$), and leading edge ($C_{m,LE}$).
- To observe and understand the working and operational procedures of a suction-type wind tunnel.
- To estimate the location of the aerodynamic center for a thin symmetric airfoil using the computed sectional lift coefficients (C_l) and pitching moments about the quarter chord point ($C_{m,c/4}$).

- To measure the pressure distribution along the surface of a symmetric airfoil and analyze incompressible flow at high Reynolds numbers.
- To capture the incompressible flow past a symmetric airfoil and calculate relevant aerodynamic properties.
- To analyze the results of flow and pressure distribution for determining the aerodynamic center.

3 Theory

3.1 Airfoil

The geometrical features of a standard airfoil are depicted in Fig. 1.

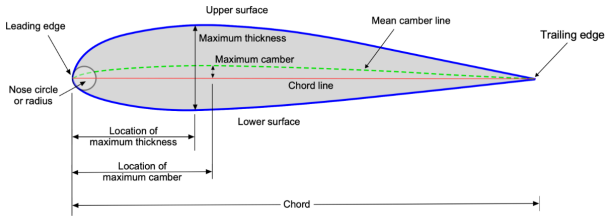

Figure 1: Airfoil Nomenclature

An airfoil is a two-dimensional profile that interacts with airflow to produce aerodynamic forces, which act both parallel (Drag in this case) and perpendicular (Lift in this case) to the flow direction. These forces are known as aerodynamic forces. The component of the net force perpendicular to the mean chord direction is called N, while the component along the free stream direction is labeled A. These forces are illustrated in Fig. 2. These are also shown in Fig. 2. .

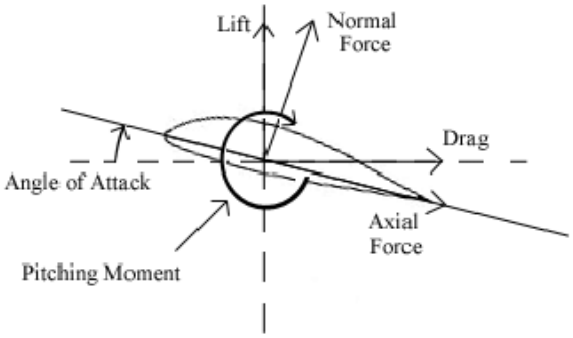

Figure 2: Aerodynamic Forces

The force components are related by the following equations:

$$L = N\cos\alpha - A\sin\alpha \tag{1}$$

$$D = N\sin\alpha + A\cos\alpha \tag{2}$$

3.2 Airfoil Geometry

Airfoil used is NACA 2412, as shown in Fig 3. The shape of an airfoil is characterized by its maximum camber (m), denoted by the first digit as a percentage of the airfoil's chord length. The location of the maximum camber (p), represented by the second digit in tenths of the chord length, and the maximum thickness (t), indicated by the last two digits as a percentage of the chord length. These parameters are illustrated in Fig. 3.

Figure 3: NACA 2412 Airfoil

Chord length (c)	150 mm
Span (b)	2 ft
Maximum thickness (% chord)	12
Maximum Camber (% chord)	2
Position of Max. Camber (% chord) (p)	40

Table 1: Characteristics Of NACA 2412

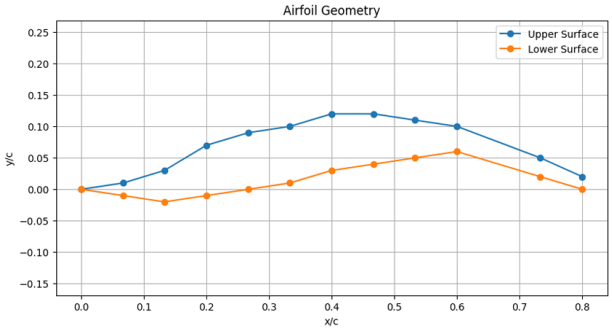

Figure 4: Airfoil with given data points

To accurately scale the airfoil shape, the chord length is required, as the notation provided only defines the shape relative to a unit chord length. The equations for the upper and lower surfaces of a NACA airfoil can therefore be expressed as:

$$z_c = \begin{cases} \frac{m}{p^2}(2px - x^2), & 0 \leq x \leq p \\ \frac{m}{(1-p)^2}\left((1-2p) + 2px - x^2\right), & p \leq x \leq 1 \end{cases} \tag{3}$$

The upper and lower surface coordinates can thus be found using the equations:

$$z_u = z_c + z_t \tag{4}$$
$$z_l = z_c - z_t \tag{5}$$

where z_t is the airfoil half thickness at a given value of x given by

$$z_t = 5t\left[0.2969\sqrt{x} - 0.1260x - 0.3516x^2 + 0.2843x^3 - 0.1015x^4\right] \tag{6}$$

The last coefficient may be replaced with -0.1036 in order to obtain a sharp, closed trailing edge without changing the overall shape of the airfoil too much.
For symmetric airfoils $z_c = 0$ and thus one only needs to obtain the thickness distribution and chord length in order to characterise the airfoil shape.

3.3 Experimental Calculations

Aerodynamic characteristics of the airfoil can be calculated using the following formula:

$$C_n = \frac{1}{c}\left[\int_0^c (C_{p,l} - C_{p,u})\,dx + \int_0^c \left(C_{f,u}\frac{dz_u}{dx} - C_{f,l}\frac{dz_l}{dx}\right)dx\right] \tag{7}$$

$$C_a = \frac{1}{c}\left[\int_0^c \left(C_{p,u}\frac{dz_u}{dx} - C_{p,l}\frac{dz_l}{dx}\right)dx + \int_0^c (C_{f,u} + C_{f,l})\,dx\right] \tag{8}$$

$$\begin{aligned} C_{m,LE} = \frac{1}{c^2}\Bigg[&\int_0^c (C_{p,u} - C_{p,l})x\,dx - \int_0^c \left(C_{f,u}\frac{dz_u}{dx} - C_{f,l}\frac{dz_l}{dx}\right)x\,dx \\ &+ \int_0^c \left(C_{p,u}\frac{dz_u}{dx} + C_{f,u}\right)z_u\,dx - \int_0^c \left(C_{p,l}\frac{dz_l}{dx} + C_{f,l}\right)z_l\,dx\Bigg] \end{aligned} \tag{9}$$

1. Since the forces due to viscous effects are smaller compared to inertial forces, we assume that the coefficients $C_{f,u}$ and $C_{f,l}$ are small compared to the coefficients $C_{p,u}$ and $C_{p,l}$ respectively.

2. Since $C_{f,u}$ and $C_{f,l}$ are assumed to be small compared to the coefficients $C_{p,u}$ and $C_{p,l}$, we neglect the second order terms in eqn. 7, 8, and 9 to obtain eqn. 10, 11, and 12 respectively. Here we are assuming the derivatives $\frac{dz_u}{dx}$ and $\frac{dz_l}{dx}$ to be finite as the airfoil does not consist of any sharp edges on the upper and lower surface.

$$C_n = \frac{1}{c}\int_0^c (C_{p,l} - C_{p,u})\, dx \tag{10}$$

$$C_a = \frac{1}{c}\int_0^c \left(C_{p,u}\frac{dz_u}{dx} - C_{p,l}\frac{dz_l}{dx}\right) dx \tag{11}$$

$$C_{m,LE} = \frac{1}{c^2}\int_0^c (C_{p,u} - C_{p,l}) x dx + \int_0^c \left(z_u C_{p,u}\frac{dz_u}{dx} - z_l C_{p,l}\frac{dz_l}{dx}\right) dx \tag{12}$$

We compute the sectional coefficients of lift and pressure drag from the expressions below:

$$C_l = C_n \cos\alpha - C_a \sin\alpha \tag{13}$$

$$C_{d,p} = C_n \sin\alpha + C_a \cos\alpha \tag{14}$$

The sectional moment coefficient about the quarter chord point will be computed as:

$$C_{m,c/4} = \frac{1}{c^2}\left[\int_0^c (C_{p,u} - C_{p,l})\left(x - \frac{c}{4}\right) dx + \int_0^c \left(z_u C_{p,u}\frac{dz_u}{dx} - z_l C_{p,l}\frac{dz_l}{dx}\right) dx\right] \tag{15}$$

The center of pressure, where the lift force is assumed to act, is computed as shown below:

$$x_{cp} \approx -\frac{M'_{LE}}{L'} \quad \text{at small } \alpha \tag{16}$$

From the velocity profile $u(z)$ in the airfoil wake, we can calculate the sectional coefficient of total drag:

$$C_{d,total} = \frac{2}{S}\left[\int_h^b \frac{u(z)}{V_\infty}\left(1 - \frac{u(z)}{V_\infty}\right) dz\right] \tag{17}$$

$$C_{d,f} = C_{d,total} - C_{d,p} \tag{18}$$

The integrals involved in above formulae are evaluated using the trapezoidal rule for integration, and the backward difference to compute derivatives as shown in the expressions below:

$$\int f(x)dx \approx \sum \frac{x_{i+1} - x_i}{2}\left[f(x_{i+1}) + f(x_i)\right] \tag{19}$$

$$\frac{df(x_i)}{dx} \approx \frac{f(x_i) - f(x_{i-1})}{x_i - x_{i-1}} \tag{20}$$

3.4 Theoretical Predictions-Using Thin airfoil theory

Thin airfoil theory is a fundamental concept in aerodynamics that explains how airfoils generate lift in incompressible, inviscid flow. It assumes airfoils to be infinitely long and thin, emphasizing the relationship between the angle of attack and lift. For symmetric airfoils, the lift coefficient C_l is given by:

$$C_l = 2\pi\alpha$$

where α is the angle of attack in radians. For cambered airfoils, this coefficient is modified to account for zero-lift conditions. The center of pressure for symmetric airfoils is located at the quarter-chord point, shifting for cambered airfoils depending on the angle of attack. Thin airfoil theory has limitations, especially in predicting stall at higher angles of attack, but it is useful for comparing and analyzing aerodynamic parameters.
Key results from Thin Airfoil Theory:

1. **Lift coefficient and its derivative with respect to angle of attack**:

$$C_l = 2\pi(\alpha + \alpha_{L=0}) \tag{21}$$

$$\frac{dC_l}{d\alpha} = 2\pi \tag{22}$$

2. **Center of pressure X_{cp}**:

$$M'_{LE} = -\frac{c}{4}N' + M\frac{\xi}{4} = -x_{cp}N' \tag{23}$$

3. **Aerodynamic center X_{ac}**:

$$\frac{dC_l}{d\alpha} = a_0 \tag{24}$$

$$\frac{dC_{m,c/4}}{d\alpha} = m_0 \tag{25}$$

$$\frac{x_{ac}}{c} = \frac{-m_0}{a_0} + 0.25 \tag{26}$$

4. **Estimating total drag and skin friction drag coefficient from velocity measurements**:

$$C_d = \frac{2}{c}\int_h^b \frac{V}{V_\infty}\left(1 - \frac{V}{V_\infty}\right)dy \tag{27}$$

$$C_{d,f} = C_d - C_{d,p} \tag{28}$$

4 Apparatus Used

1. NACA 2412 airfoil (with pressure ports for pressure measurement).

2. Wind Tunnel
3. Pitot static probe
4. 2 channel selector boxes
5. Spirit level (angle setter)
6. Digital Manometer
7. Traverse (horizontal and vertical)

4.1 Wind Tunnel

The wind tunnel used is an open-channel suction-type wind tunnel. Two-dimensional flow effects are mitigated by installing bell mount structures at the tunnel's inlet. Screens are positioned upstream of the inlet to homogenize turbulence effects and prevent eddy formation as the flow enters the tunnel. For this purpose, one horizontal screen and one netted screen are utilized. The flow is accelerated through a 9:1 converging nozzle, and the desired speed is achieved by adjusting the motor RPM. Care is taken to position measurement devices away from the walls to ensure that the flow is uniform and quasi-one-dimensional. After passing through the test section, the flow is decelerated through a diffuser before exiting through the fan manifold.

5 Experimental Setup

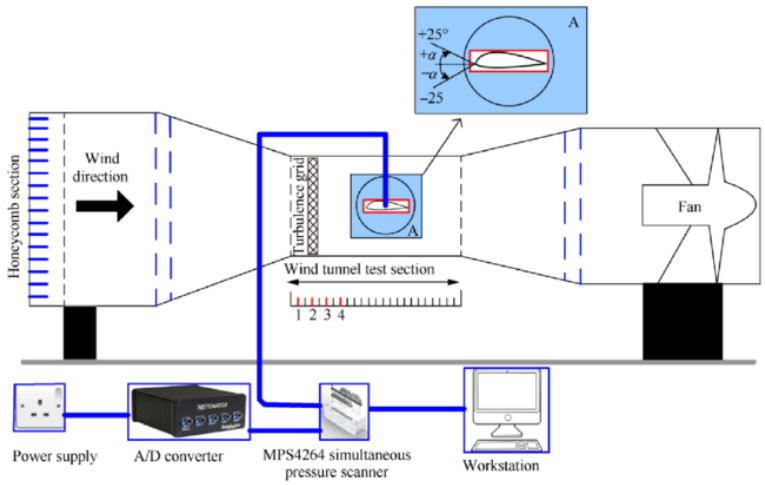

Figure 5: Experimental Setup

6 Theoretical Assumptions

1. The fluid (air) is assumed to be in the continuum regime, with all properties considered to be point-wise continuous, as per the Continuum Hypothesis.

2. The flow past the airfoil is assumed to be predominantly influenced by inertial effects rather than viscous effects (momentum diffusion). This assumption is validated by the large Reynolds number (Re = 219137.10).

3. The airfoil is considered to have a small thickness, thereby minimally perturbing the flow. This is evident from the fact that the maximum thickness is only 12% of the chord length in this particular experimental setup. This simplifies the expressions for axial and normal force coefficients, as we can neglect the second-order terms in Eqn. 8.

4. The flow past the airfoil is assumed to be within the incompressible regime, as the Mach number of the flow is small (M = 0.0504). This assumption facilitates the simplification of conservation laws for mass and momentum into the equations.

5. Integrals computed using the trapezoidal rule are considered to be reasonably accurate.

7 Procedure

7.1 Ambient Data and Associated Errors

Param	**Measured Value**	**Abs Error**
T_∞	300.15 K	0.1 K
P_∞	100010 Pa	10 Pa
ρ_∞	1.198 $kg/m^3$3	0.0075 kg/m3
$V_{\infty,\text{test}}$	17.5 m/s	0 m/s

Table 2: Measured Values and Absolute Errors for Day-1

7.2 Measurement of Airfoil Surface Pressure Distribution

1. Ambient conditions, including temperature and pressure, are recorded to calculate air density and the corresponding dynamic pressure for the specified velocity.

2. The wind tunnel and airfoil are inspected for leaks and clogged ports; any identified leaks are sealed, and data from clogged ports are ignored.

3. The motor frequency is set to achieve the required dynamic pressure, as measured by a Pitot probe, and remains undisturbed thereafter.

4. Pressure readings are obtained from 28 tubes connected to the airfoil's pressure ports, and the required angle of attack is set using a spirit level to ensure accuracy.

5. Gauge pressure is recorded for each port at angle of attack -5°, -3°, -1°, 0°, 1°, 2°, 3°, 5°.

7.3 Measurement of Airfoil Wake Velocity Profile

1. The Pitot tube is positioned behind the airfoil, above its immediate wake, by moving it along the x-direction using a traverse system.
2. The Pitot tube is inspected to ensure it is properly aligned with the free stream flow direction.
3. The Pitot tube is adjusted along the y-direction in small increments, recording value of the dynamic pressure head at each y-location to ensure repeatability.
4. The above measurements are repeated for various angles of attack, ranging from -3°, 0°, 3°.

8 Plots

8.1 C_p Plots

For $\alpha = 0$ °

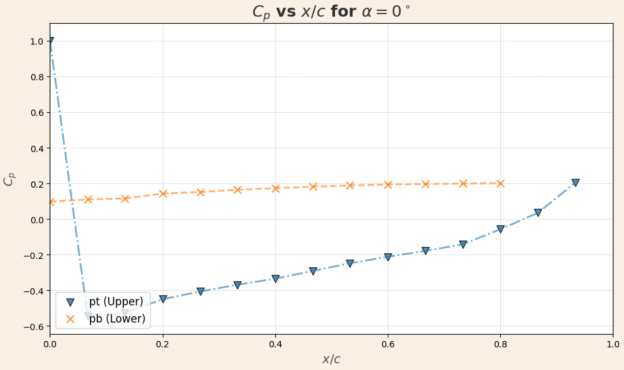

For $\alpha = 1$ °

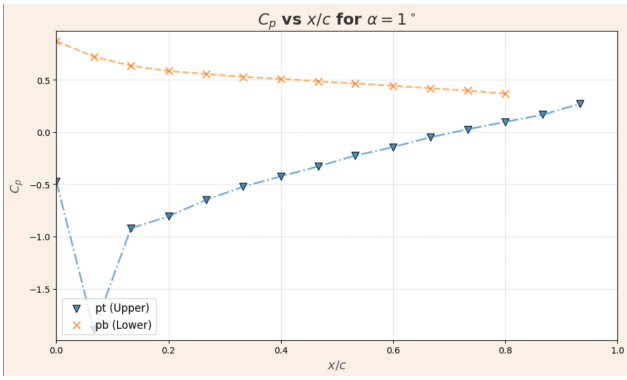

For $\alpha = 3$ °

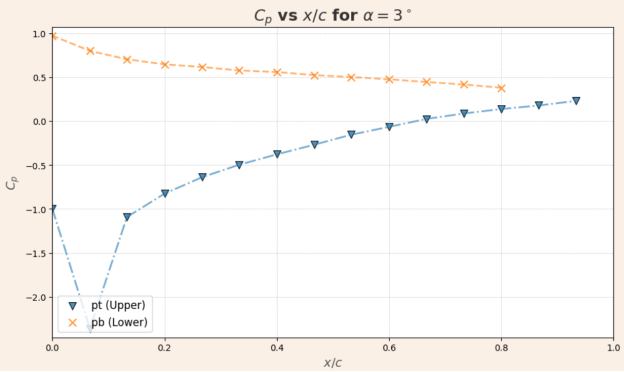

For $\alpha = 5^\circ$

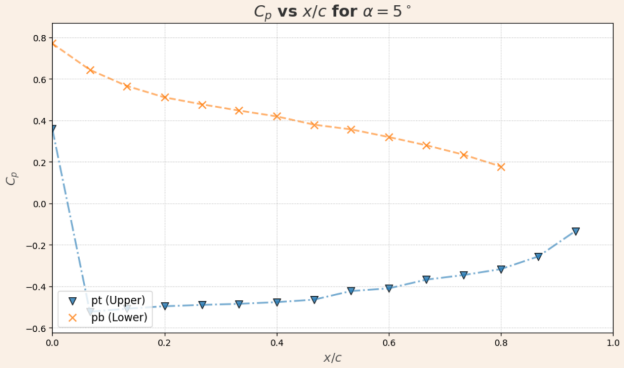

For α = -1 $^\circ$

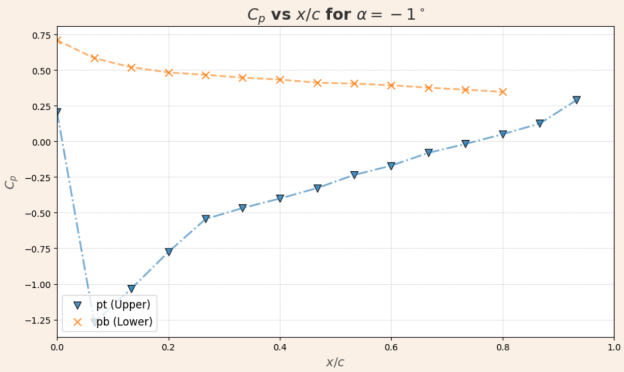

For α = -3 $^\circ$

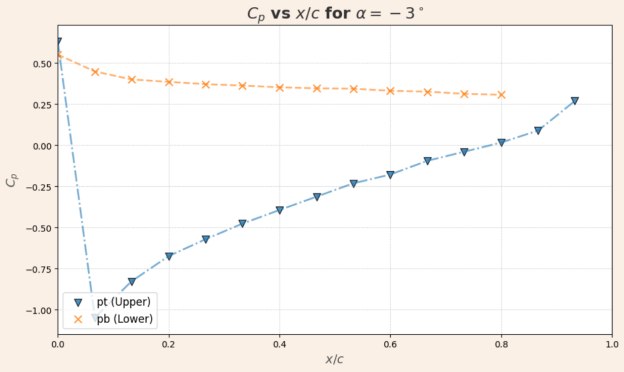

For α = -5 °

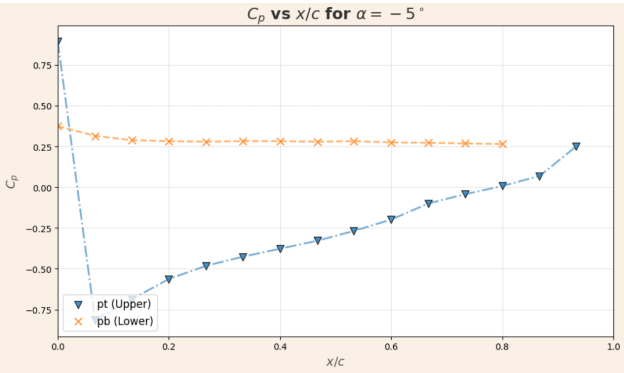

8.2 Wake Velocity Profile

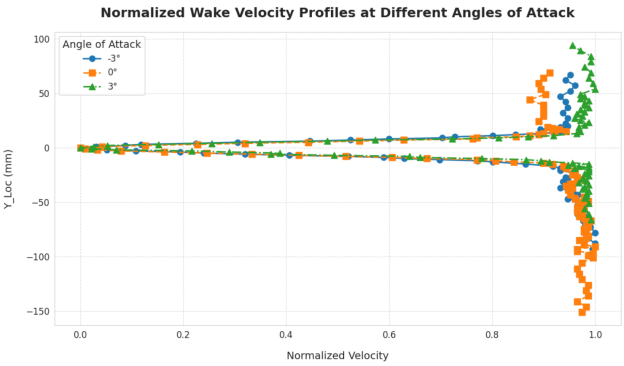

Figure 6: Wake Velocity for different values of α

8.3 C_L vs α

The plots for C_l versus α obtained from the wind tunnel are shown in Figure 8.3. These results are compared with the theoretical values, calculated using Equation 29 from Thin Airfoil Theory, and with data obtained from the computational software **XFLR5**.

$$C_{l_{theo}} = 2\pi \left[\alpha + \frac{1}{\pi} \int_0^{\pi} \frac{dz}{dx} \left(\cos(\theta_0) - 1 \right) d\theta_0 \right] \tag{29}$$

$$\Rightarrow C_{l_{theo}} = 2\pi[\alpha], \text{ where } \alpha \text{ is in radians} \tag{30}$$

$$\Rightarrow C_{l_{theo}} = 0.1097\alpha, \text{ where } \alpha \text{ is in degrees} \tag{31}$$

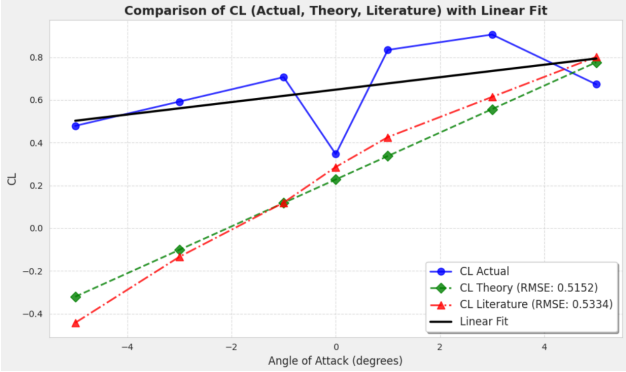

8.4 C_d - Pressure, Skin friction, Total vs α

The plots of $C_{d,\text{pressure}}$, $C_{d,\text{skin friction}}$, and $C_{d,\text{total}}$ versus α, obtained from the wind tunnel, are shown in Figure 7, Figure 8, and Figure 9, respectively. These results are compared with the numerical values obtained from the software **XFLR5**. Since the theoretical drag calculation requires detailed knowledge of the theoretical pressure distribution in the airfoil wake, it is omitted in this analysis. Instead, validation is performed for $\alpha = 0°$ using similar Reynolds number data from the literature.

Pressure Drag:

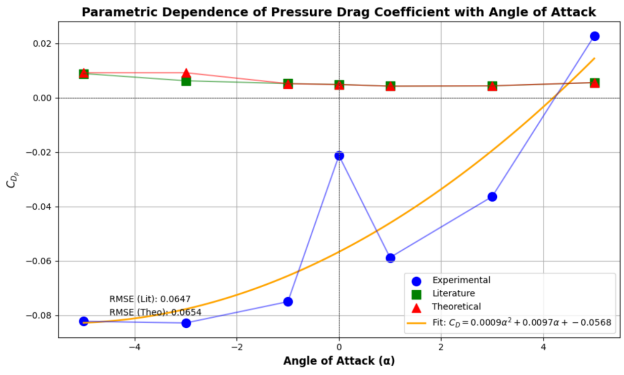

Figure 7: Pressure Drag vs α

Skin Friction Drag:

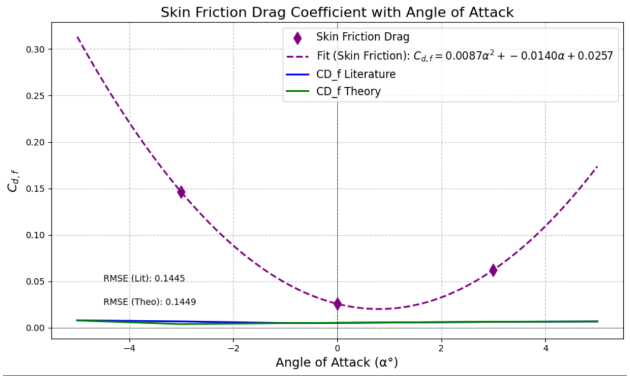

Figure 8: Skin Friction Drag vs α

Total Drag:

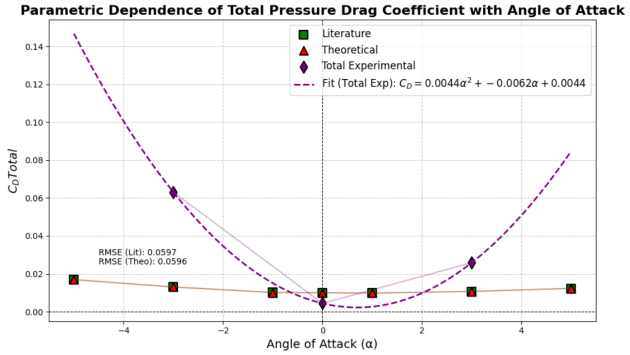

Figure 9: Total Drag vs α

8.5 C_m - LE, c/4 vs α

Moment Coefficient-LE

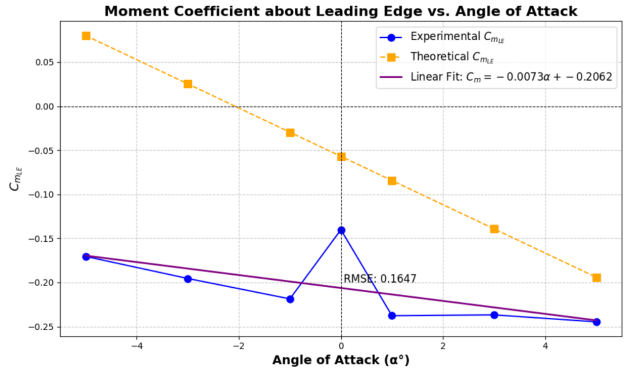

Figure 10: C_{mLE} vs α

Moment Coefficient-c/4

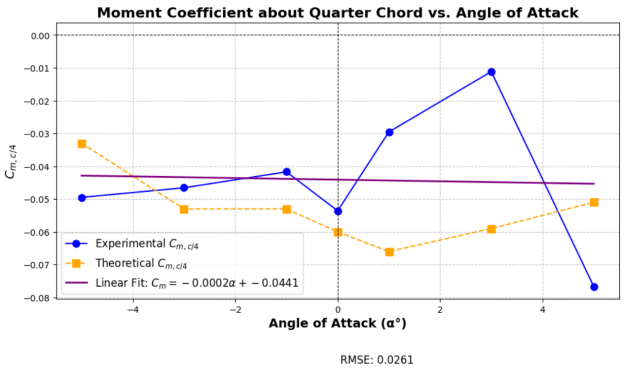

Figure 11: $C_{mc/4}$ vs α

8.6 X_{cp} vs α

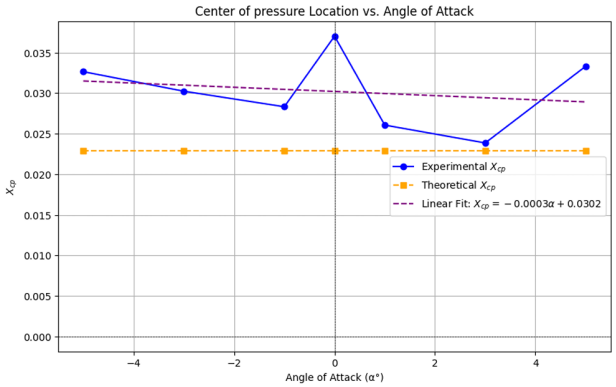

9 Experimental Calculations

9.1 Sample Calculation approach

Using the C_p distribution obtained from the wind tunnel experiment and the airfoil coordinates corresponding to the pressure port locations, the axial and normal force coefficients (sectional) are computed using Eqs. 10 and 11.

The sectional lift and pressure (form) drag coefficients, as well as the leading edge moment coefficient, are derived from the axial and normal force data using Eqs. 12, 13 and 14.

Note: The simplification of the expressions for lift and drag coefficients for small incidence angles is not applied for higher accuracy.

The sectional moment coefficient about the quarter-chord point and an estimate of the aerodynamic center are calculated using Eqs. 15 and 16.

Using the velocity profile in the airfoil wake, the sectional total drag coefficient is computed using Eq. 17.

From the computed sectional pressure and total drag coefficients, the skin-friction drag

coefficient is determined as follows:

$$C_{d,f} = C_{d,total} - Cd, p \tag{32}$$

9.2 Tabulated Calculations

$\alpha(^\circ)$	-5	-3	-1	0	1	3	5
$C_{l,\text{theor}}$	-0.320	-0.101	0.177	0.227	0.337	0.556	0.775
$C_{l,\text{exp}}$	0.478	0.592	0.706	0.346	0.833	0.905	0.672
$C_{m\text{LE,theor}}$	0.080	0.025	-0.029	-0.056	-0.084	-0.139	-0.193
$C_{m\text{LE,exp}}$	-0.170	-0.195	-0.218	-0.140	-0.237	-0.236	-0.244
$C_{m\frac{c}{4},\text{theor}}$	-0.033	-0.053	-0.053	-0.06	-0.066	-0.059	-0.051
$C_{m\frac{c}{4},\text{exp}}$	-0.049	-0.046	-0.041	-0.053	-0.029	-0.011	-0.076
$x_{cp,\text{theor}}$	0.105	0.101	0.094	0.110	0.077	0.052	0.142
$x_{cp,\text{exp}}$	0.124	0.177	0.001	0.178	0.066	-0.182	-0.028

Table 3: Experimental and theoretical data

$\alpha(^\circ)$	-5	-3	-1	0	1	3	5
$C_{d,\text{total (XFLR5)}}$	0.016	0.013	0.010	0.010	0.009	0.010	0.012
$C_{d,\text{total}}$	-	0.063	-	0.004	-	0.025	-
$C_{d,\text{pressure (XFLR5)}}$	0.009	0.006	0.005	0.004	0.004	0.004	0.005
$C_{d,\text{pressure}}$	-0.08	-0.08	-0.07	-0.02	-0.05	-0.03	0.02
$C_{d,\text{skin friction (XFLR5)}}$	0.007	0.007	0.005	0.006	0.005		0.007
$C_{d,\text{skin friction}}$	-	0.143	-	0.024	-	0.055	-

Table 4: Drag coefficient Comparison with XFLR5 data

10 Stall angle and Aerodynamic Center location estimation

10.1 Stall Angle

The data appears unreliable as it shows a dip in the lift coefficient C_L at an angle of attack of 0 degrees, and the C_L values are higher than both theoretical predictions and values found in the literature. According to the experimental data, there is a noticeable drop in C_L at 5 degrees, as seen in Figure 14. This could be interpreted as the stall angle; however, due to the inaccuracy of the data, theoretical and literature values are preferred. The angle at which C_L begins to decrease is determined to be 14.5 degrees. Here is the picture:

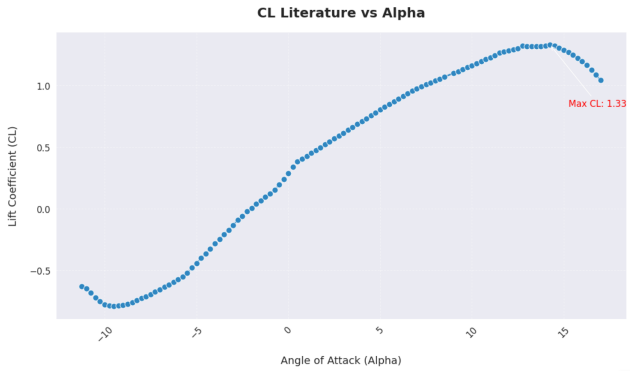

Figure 12: C_L vs α-Data taken from NACA Website

10.2 AC Location Estimation

The aerodynamic center is estimated both theoretically and using experimental data, using equations 24, 25 and 26. The theoretical calculation gives a value of 0.0378 m, while the experimental data yields a value of 0.0464 m. These estimates are derived using the slope of C_L and $C_{m,c/4}$ from the experimental and theoretical data, respectively.

11 Error

11.1 Source of Error

The following are the sources of errors due to the least count of measurement devices:

1. The barometer has an error of 0.01 millibars (4 significant digits).
2. The thermometer has an error of 0.1 K (3 significant digits when expressed in Kelvin).
3. The manometer carries an error of 0.1 pascal (3 significant digits).
4. The screw gauge used for obtaining airfoil coordinates has an error of 10 µm (2 significant digits for the y-coordinate in mm, and 4 significant digits for the x-coordinate in mm).

11.2 Error Analysis

We use the following relations for error analysis and propagation of arithmetic errors:

$$z = x + y \tag{33}$$

$$\Delta z = \sqrt{(\Delta x)^2 + (\Delta y)^2} \tag{34}$$

$$z = x * y \ or \ x/y \tag{35}$$

$$\frac{\Delta z}{z} = \sqrt{\left(\frac{\Delta x}{x}\right)^2 + \left(\frac{\Delta y}{y}\right)^2} \tag{36}$$

- The C_L value at a 0-degree angle is lower compared to other values, while other C_L values appear shifted upward relative to the theoretical data. This discrepancy may be due to human error, as the C_p values, calculated using dynamic pressure from port values, fluctuate significantly within the range of 2 to 5 SI units.

- Another error stems from the reference temperature R being taken as 278 K, whereas it should be 287 K. Although this change may not drastically affect the velocity, it still contributes to the overall error.

- Errors may also arise from the methods used to calculate aerodynamic parameters such as C_L and C_D.

- The integration is limited to specific points on the airfoil, with 15 points on the top and 13 on the bottom.

- The integration process sometimes involves algebraic derivatives such as $\frac{dy}{dx}$ or $\frac{dz}{dx}$, which may have large deviations, contributing to significant errors, as seen in the plots of the airfoil ports from which dynamic pressure was calculated.

- Taking $C_p = \frac{P}{0.5 \times \rho V_\infty^2}$, the relative error in ρ is 20.2×10^{-2}. Thus, the relative error in C_p is $\pm 18.2 \times 10^{-2}$.

- According to the respective calculations, the relative error in C_a and C_n is approximately 18.7×10^{-2}.

- The relative error that propagates to C_L is approximately 20.2 for the case of $\alpha = 0$ and about 20.3×10^{-2} assuming that α is taken to 4 significant digits or more in other cases.

- Similarly, the error in $C_{m,LE}$ is $\approx 20.97 \times 10^{-2}$, and the error in $C_{m,c/4}$ is $\approx 11.86 \times 10^{-2}$.

- The percentage error between the calculated values of the aerodynamic center and the predicted values from Thin Airfoil Theory comes out to be 38.5%.

12 Tabulated dependence on α and RMS Error

Quantity	Parametric dependence on α	RMSE
C_l	0.1041 α	0.5152
$C_{d,pressure}$	0.0012 α^2 -0.0013 α + 0.0329	0.0647
$C_{d,Skinfriction}$	0.0002 α^2 -0.0019 α + 0.0561	0.1449
$C_{d,total}$	0.0014 α^2 -0.0005 α + 0.0889	0.0596
$C_{m,LE}$	-0.0330 α	0.1647
$C_{m,c/4}$	-0.0286 α	0.0261
X_{cp}/C	-0.0063 α + 0.2621	0.0084
X_{ac}/C	Assumed independent of α	0.0086

Table 5: Table for parametric dependence on α and RMSE

13 Conclusion and Discussion

- **Aerodynamic Center Location**: The aerodynamic center was found at approximately $0.22X_c$, which is near the quarter-chord prediction. However, discrepancies highlight the limitations of Thin Airfoil Theory in predicting real airfoil performance, especially at higher angles of attack.

- **Moment Coefficient Trends**: The measured values of $C_{m,LE}$ and $C_{m,c/4}$ generally align with data from AirfoilTools, though deviations from linearity are observed due to airfoil thickness and flow disturbances. These deviations become particularly noticeable at higher angles of attack.

- **Pressure Head Trends**: As flow incidence angles increase, the pressure head on the suction surface rises in accordance with theoretical expectations. Additionally, the reversal of suction and pressure surfaces at negative angles mirrors established aerodynamic principles.

- **Lift Coefficient Discrepancies**: Measured lift coefficients diverge significantly from those predicted by Thin Airfoil Theory, especially at higher angles of attack. These differences emphasize the theory's limitations, particularly when airfoil thickness becomes a more prominent factor.

- **Velocity Profile Accuracy**: Experimental velocity profiles closely match reference data from the literature, with minor discrepancies that are likely due to tunnel leakage. The data supports the expected trends, such as higher angles of attack leading to increased wake velocities and longer wake lengths.

- **Faulty Sensor Data**: Certain faulty pressure sensor readings were identified and discarded. This adjustment led to better accuracy in C_p distribution plots, which now align more closely with theoretical predictions.

- **Center of Pressure Observations**: While the experimental X_{cp} values are generally in line with theoretical predictions, anomalous behavior is observed at a zero angle of incidence. This can be attributed to the characteristics of symmetrical airfoils, where X_{cp} becomes indeterminate.
- C_p **Data Analysis**: C_p data matches Thin Airfoil Theory predictions at $\alpha = 0$, but deviations appear at higher angles of attack. These deviations reveal the theory's inability to accurately model the behavior of thicker airfoils across different flow conditions.
- **Discrepancies in Wake Profiles**: There are some differences between the measured wake profiles and theoretical predictions, particularly at high angles of attack. These deviations highlight the influence of airfoil thickness and surface irregularities on wake development.

14 References

- Figure 1
- Figure 2
- NACA 2412 Airfoil
- Experimental Setup
- Excel Sheet
- Google Colab
- Lecture Slides of Prof. Vineet Nair